Materials Research Proceedings 54 (2025) 936-945 https://doi.org/10.21741/9781644903599-100

Forging of hybrid gears with wear-resistant surfaces using deposition-welded semi-finished products

Niklas GERKE[1,a *], Laura BUDDE[2,b], Eduard ORTLIEB[1,c], Simon PEDDINGHAUS[1,d], Kai BIESTER[2,e], Julius PEDDINGHAUS[1,f], Hendrik WESTER[1,g], Johanna UHE[1,h], Jörg HERMSDORF[2,i], Nick SCHWARZ[2,j], Ludger OVERMEYER[2,k] and Bernd-Arno BEHRENS[1,l]

[1]Leibniz University Hannover, Institute of Forming Technology and Machines, An der Universität 2, 30823 Garbsen, Germany

[2]Laser Zentrum Hannover e. V., Hollerithallee 8, 30419 Hannover, Germany

[a]gerke@ifum.uni-hannover.de, [b]l.budde@lzh.de, [c]ortlieb@ifum.uni-hannover.de, [d]s.peddinghaus@ifum.uni-hannover.de, [e]k.biester@lzh.de, [f]peddinghaus@ifum.uni-hannover.de, [g]wester@ifum.uni-hannover.de, [h]uhe@ifum.uni-hannover.de, [i]j.hermsdorf@lzh.de, [j]n.schwarz@lzh.de, [k]l.overmeyer@lzh.de, [l]behrens@ifum.uni-hannover.de

Keywords: Die forging, Laser Hot-Wire Cladding, Hybrid Components, Tailored Forming, Directed Energy Deposition

Abstract. New technologies are needed to keep up with the increasing demand for high-performance components. One approach is to forge hybrid components from prefabricated multimaterial billets (Tailored Forming). This work focuses on the material distribution after a die forging process investigating the example of a hybrid spur gear. Different layer thicknesses of the material X45CrSi9-3 were applied to a blank made of C22.8 using a laser hot-wire cladding process. The semi-finished products were then hot-formed into near-net-shape spur gears. In order to investigate the influence of different cladding thicknesses on the material distribution across the tooth geometry after hot forging, metallographic sections were analyzed. The joining zone microstructure was analyzed for defects and hardness measurements were carried out. In addition, FEM was used to simulate how different layer thicknesses of a cladded blank affect the material distribution in forming. The results of the numerical and experimental analysis showed that the resulting material distribution can be predicted with high precision using FE process modeling.

Introduction

Mono-materials are generally used to manufacture components such as spur gears using conventional forging and machining processes. Often, a compromise is made between the properties of the material and the economic requirements. Increasing requirements regarding components mechanical properties result from current trends towards resource and energy efficiency [1]. Mono-materials are however reaching their limits. For that reason, hybrid materials are becoming increasingly relevant. By combining different materials, local requirements for high-performance components in relevant sections can be met and the efficiency can be increased [2]. Such concepts are already being implemented in sheet metal production and processing with tailored blanks [3] or platinized rolling [4]. Comparable processes are not yet established in hot bulk forming, which is why attempts are being made to close this research gap with innovative, customized forming process chains. This is being done in the Collaborative Research Center 1153. Process chains for the production of hybrid metallic high-performance components through hot or warm forming of previously joined preforms by Tailored Forming are being investigated.

State of the art

During use different load conditions prevail locally in different areas of a gearwheel. Those conditions are bending in the tooth root and a rolling load under high local pressure on the tooth flank. Such loading conditions results in two significant damage mechanisms. Crack nucleation at the tooth root and wear at the tooth flank. High hardness is advantageous against wear and high ductility against cracking. These approaches are however counteracting. In order to maintain ductility in the tooth root, only the tooth flanks are induction hardened locally. The achievable hardness is limited by the material. Finally, the gears are hard-machined to their final dimensions [5]. Another method of local adaptation of properties is through multi-material design. Results by Wang et al. towards forge bonding show that the material interface is critical. The approach chosen in this paper addresses that issue by cladding a billet through deposition welding to generate a sufficient material bond prior to forming [6].

A series of studies were carried out on the production of hybrid bevel gears using the Tailored Forming process chain. The combination of materials allows an increase of hardness in the tooth flank without compromising the ductility and crack resistance in the root. These consist of a substrate made of C22.8 with claddings of 41Cr4 [7, 8] or X45CrSi9-3 [8, 9, 10], which were applied using plasma transferred arc welding or laser hot-wire cladding. For the laser hot-wire cladding process, the additional material is fed in form of a wire and melted by the laser beam. An electric current through the wire between welding nozzle and substrate leads to conductive heating of the wire and thus to a reduction in the laser power required to melt and bond the wire. The wire preheating also allows an increase of the deposition rate [11, 12]. The hybrid semi-finished parts were successfully formed into bevel gears without layer separation. The hardness of the 41Cr4 cladding was in the range of 275 HV 0.1 after deposition welding and decreased to 200 HV0.1 to 250 HV 0.1 after hot forming [7]. The lower cooling rates after hot forming were assumed to be the cause. To achieve the desired hardening mechanical properties and microstructure with high wear resistance in the cladding layer, a process-integrated heat treatment by quenching and subsequent self-tempering in an air-water spray field was developed [8, 9]. The heat treatment improved the tensile strength of the hybrid bevel gears and caused a significant increase in hardness of the cladding material. Hardness values of up to 513 HV 0.5 were achieved after heat treatment in the 41Cr4 cladding while the X45CrSi9-3 cladding reached 732 HV 0.5. A direct comparison of the hardness values is not possible due to the different test loads and the associated penetration depth and test area. Nevertheless, qualitative tendencies can be shown.

Aim of the investigations

For an efficient application of Tailored Forming for gear components, a load adapted material distribution is necessary. In order to optimize this distribution, the influence of initial billet cladding thickness on the material flow must be characterized and modelled. This work aims to provide a baseline for this through an experimental investigation of material flow for different layer thickness and a validation of a multi-material FE process model.

Materials and methods

In the following sections, the materials and processes used for laser hot-wire cladding and die forging are described. Furthermore, the analytical methods and the simulation tools are presented.

A cylindrical blank is used as the substrate. Four different cladding thicknesses between 1.5 mm and 7.5 mm are considered in this investigation. The outer diameter of the hybrid semi-finished product after cladding must be 65 mm, to be able to compare the effects of the different layer thicknesses on the material flow and distribution. The substrate diameter is therefore adapted to the cladding thickness. An overview of the substrate diameters used and the corresponding cladding thicknesses is shown in Table 1. The target geometry of the finished component corresponds to an FZG test gear of form A with 16 teeth, a pressure angle of 20 ° and a module of 4.5 mm.

Materials
Unalloyed structural steel C22.8 with an initial hardness of 165 ± 12 HV is used as the substrate material. The cladding consists of the martensitic steel X45CrSi9-3, which is characterized by its high hardness and good weldability [14] and an initial hardness of 718 ± 18 HV. The chemical composition of substrate and cladding material is shown in Table 2.

Table 1 – Overview of substrate diameters and cladding thickness

Substrate diameter in mm	Cladding thickness in mm
50	7.5
55	5.0
60	2.5
62	1.5

Table 2 – Chemical composition in wt. % of X45CrSi9-3 [14] and C22.8 [13]

	Fe	C	Si	Mn	P	S	Cr	Ni	Mo
C22.8 (1.0460)	Bal.	0.18 - 0.23	< 0.40	0.30 - 0.90	< 0.025	< 0.015	≤ 0.30	< 0.3	≤ 0.08
X45CrSi9-3 (1.4718)	Bal.	0.4 - 0.5	2.7 - 3.3	< 0.6	< 0.04	< 0.03	8.0 - 10.0	< 0.5	

Die forging and Analyses
The cladded samples were machined to a diameter of 64 mm and a height of 56 mm before forming. By machining, surface waviness originating of the cladding process is reduced and an even diameter ensured that enables a homogenous initial state for the material flow.For the following forming operation, the samples were heated at 1200 °C for 30 minutes. The samples were then automatically transferred into the die using an industrial robot. The tool system schematic, which is shown in Fig. 1, consists of a lower part, which contains the die for the target outer gear geometry, an ejector system, and an upper part, which consists of the punch and a closing ring, for flashless forming. The tools were not preheated.

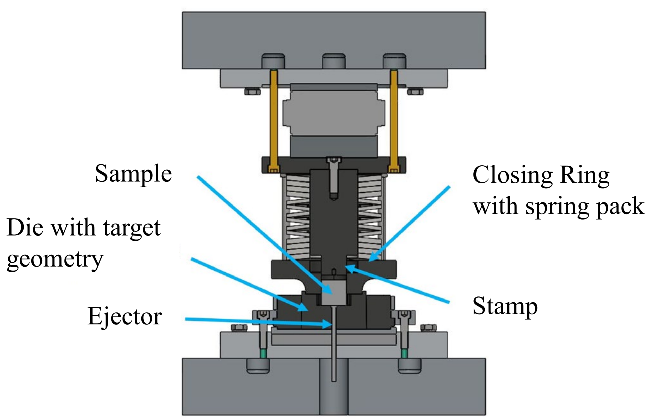

Figure 1 – Tool for manufacturing of spur gears

The nominal geometry of the toothing in the die is designed to allow machining to final dimensions after the forming process and is 91.5 mm in outer diameter. After forming, the component is lifted out of the die by the ejector and removed manually. The tool system was applied in a SPR500 screw press by LASCO Umformtechnik GmbH. A forming energy of 20 kJ was set. The forming stroke is limited by mechanical stops which absorb the excess energy. This ensures identical forming stroke for each test. Before forming, the lubricant CON TRAER G 300 from Fuchs Lubricants Germany GmbH is applied manually to all active die components. The gears are quenched directly after forming

Metallographic analyses and hardness measurements are carried out to characterize and compare the martial distribution and microstructure. For the investigations, samples were cut out of the formed semifinished spur gears using wet cut-off grinding (Fig. 2 a, b).

For the metallographic examination, the samples were treated with a nitric acid solution and then photographed using reflected light microscopy. The Vickers hardness measurement (HV 1) shown in Fig. 2 c, is carried out in the tooth tip (line length: 12 mm) and tooth root areas (line length: 4 mm) in a radial direction from the edge to the center of the sample. A further series of measurements is carried out in the center of the tooth flank orthogonally to the tooth surface (line length: 3.5 mm). The point spacing is 0.5 mm for all measurements.

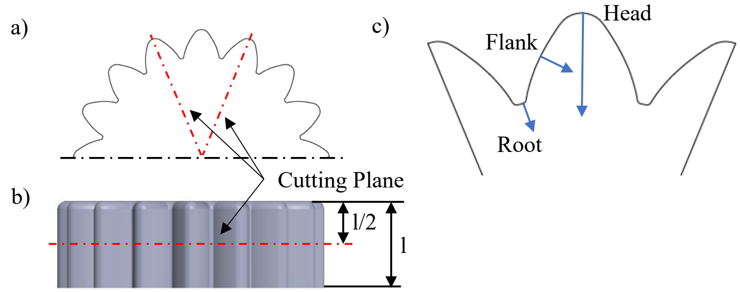

Figure 2 – Cutting plane (a, b), Course of hardness measurement (c)

Material modelling and forming simulation

The material model for X45CrSi9-3 was taken from a previous study [15], where uniaxial compression tests were carried out with the mono-material. For the C22.8 material model uniaxial compression tests were carried out on a Gleeble 3800-GTC forming. The tests were carried out at 900 °C, 1050 °C and 1200 °C using cylindrical specimens with a diameter of 10 mm and a height of 15 mm. Strain rates of 0.1 s^{-1}, 1 s^{-1} and 10 s^{-1} were investigated. Flow curves were extracted from the experimental data and a Hensel-Spittel-10 flow curve approach was fitted by a least-squares optimization algorithm. In Eq. 1, the Hensel-Spittel-10 approach is shown.

$$\sigma_f = A * e^{m_1 * T} * T^{m_8} * \varphi^{m_2} * e^{\left(\frac{m_4}{\varphi} + m_6 * \varphi\right)} * (1 + \varphi)^{(m_5 * T)} * \dot{\varphi}^{(m_3 + m_7 * T)}, \quad (1)$$

Here, the flow stress σ_f depends on the temperature T, the plastic strain φ, the strain rate $\dot{\varphi}$ as well as the materialspecific constants A and m1 to m8. Using the fitted Hensel-Spittel-10 material model, the flow behaviour can be described consistently in dependence of the strain, strain rate and temperature within numerical simulations. The determined parameters are presented in Table 3.

Table 3 shows the measured flow curves and the corresponding fitted model for different temperatures and strain rates. The fit has an r^2-Value of 0.96 and is in good agreement with the measurement data.

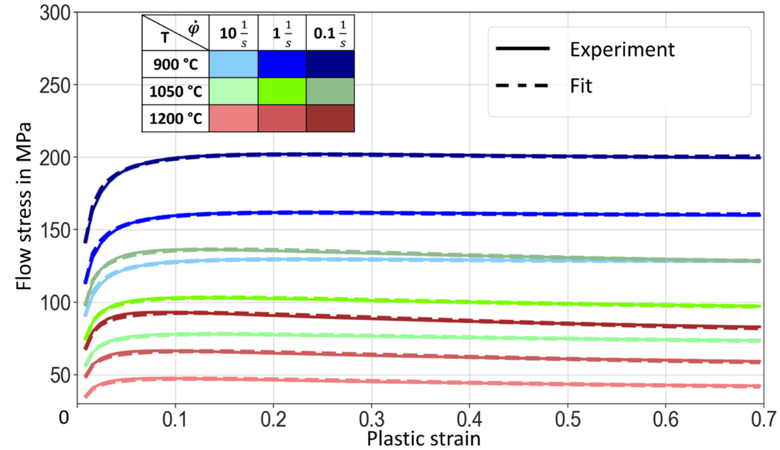

Figure 3 – Experimental and fitted flow curves for C22.8

Table 3 – Hensel-Spittel-10 parameter for C22.8

Parameter	Value
A	2443.17
m1	-0.0028402
m2	0.0477092
m3	-0.0531006
m4	-0.0022666
m5	-0.0009753
m6	0.462005
m7	0.000166
m8	-0.0005199

Finite element software simufact forming v16 was used to implement the Hensel-Spittel-10 model. To verify the material model, additional uniaxial compression tests were carried out at 1100 °C with a strain rate of 1 s^{-1} whilst keeping the same boundary conditions as for the initial experiments. The experimental setup was recreated through a numerical simulation of the compression test with the implemented model. The punch force in relation to the displacement was determined through the simulation and compared to the measured results. As shown in Fig. 4, the results of the simulation and the experiment are in good agreement with an root mean square error of 0.6396kN, therefore the resulting material model was used in the following parameter study.

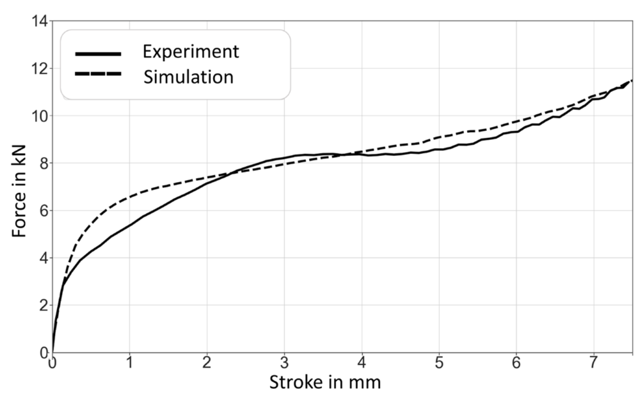

Figure 4 – The force-displacement curve determined through the simulation in comparison to the experiment

The simulation model for the parameter study of the layer thickness, as shown in Fig. 5, consists of an upper tool, a lower tool, a punch and the hybrid semi-finished product. Symmetry axes were

Materials Research Proceedings 54 (2025) 936-945 https://doi.org/10.21741/9781644903599-100

used within a 3D-model, so only a 45° section of the setup was computed to save computing time whilst still including a complete gear tooth as well as two half teeth. The tools were modelled as rigid bodies with a temperature of 20 °C to analyze the feasibility of the process in the first step. In order to model the effect of the deposition welding the substrate and cladding were modeled as distinct deformable bodies with an adhesive contact condition, ensuring that the contact nodes between the two materials adhere to each other. To investigate varying cladding thickness, geometries with the corresponding dimensions were used. The bodies were initially meshed with tetrahedral elements, which had a size of 2.5 mm. As the process shows significant plastic strain, a strain dependent remesh criteria at 0.4 was defined. To ensure precise numerical predictions, an additional refinement box was added in the area of the gear tooth, in which the element size was 1.25 mm. The initial temperature is set to be homogeneous at 1100 °C for both the C22.8 and the X45CrSi9-3. A friction model incorporating both Coulomb and viscous friction was employed, with a friction coefficient (μ) of 0.08 and a friction factor (m) of 0.3, as described in [15].

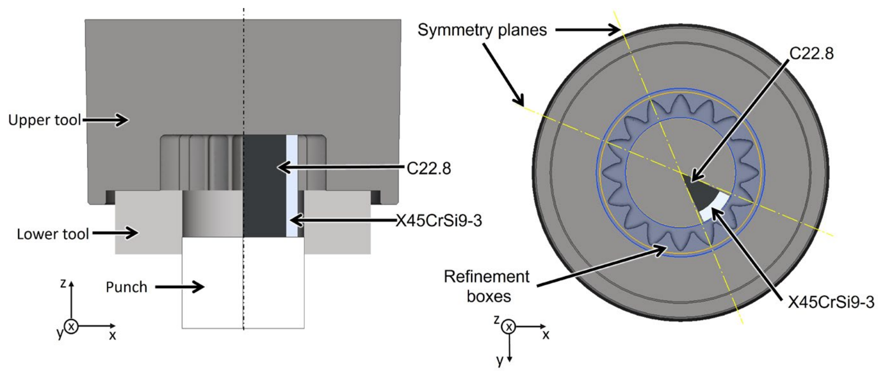

Figure 5 – a) Cross section of the simulation model b) Symmetry planes of the reduced model

Laser hot-wire cladding

For the laser hot-wire cladding process, a coaxial laser deposition welding head developed by Laser Zentrum Hannover e. V. and a LDM3000-40 diode laser beam source by Laserline GmbH is used. The substrates are sandblasted and cleaned with ethanol before being mounted on a rotational axis. Spiral weld seams are applied to the substrate. In order to achieve different cladding thicknesses, multiple layers are deposited. An overview of the parameters for the different cladding layers is given in Table 4. The parameter used for the first cladding layer for all substrate types and subsequent layers of substrates with 62 mm and 60 mm diameter are derived from previous investigations [16, 17]. Slight adjustments of the process parameters were necessary due to the change in substrate geometry. The two additional process parameter sets were determined through a small parameter study. No cracks or bonding defects were observed in cross-sections of the cladded samples examined after laser hot-wire cladding. The cladding of the substrates with a diameter of 60 mm consists of three layers, while two layers were necessary for the 62 mm substrates. For the substrates with the smaller diameter of 50 mm and 55 mm eight and five cladding layers were used to achieve sufficient cladding thickness (see Table 1).

Materials Research Proceedings 54 (2025) 936-945 https://doi.org/10.21741/9781644903599-100

Table 4 – Welding parameter for laser hot-wire cladding X45CrSi9-3 on C22.8

Parameter	Unit	First layer D50/D55/D60	Next layers D50/D55	Next layers D60	Final layer D60/D55	All layers D62
Welding speed	mm/min	1200	1800	1200	1200	1200
Current	A	100	140	100	60	100
Laser power	kW	1.65	1.50	1.65	1.50	1.65
Wire feed rate	m/min	2.0	3.0	2.0	1.0	2.0
Shielding gas flow rate (argon)	l/min	8.0	8.0	8.0	8.0	8.0
Stickout	mm	7.7	7.7	7.7	7.7	7.7
Seam-to-seam offset	mm	1.2	1.2	1.2	1.2	1.6
Laser spot	mm	2.8	2.8	2.8	2.8	2.8

Results and discussion

Following, the results of the material flow for different cladding thicknesses are presented and discussed. Afterwards, these results are compared with the FE simulation.

As shown in Fig. 6, the material distributions show clear differences with different cladding thicknesses. A significant thinning can be seen on the tooth flank in Fig. a. As the material flows into the tooth, it increases in surface area, which leads to a thinning of the surface layer. In Fig. 6 b (5 mm) and c (7.5 mm), this effect is less pronounced or not observed at all. The material of the cladding layers fills the tooth before base material can flow into the tooth and thinning occurs. Fig. 6 c shows cracks in the cladding that run along to the base material and also through the joining zone (red marking (3)). With a layer thickness of 7.5 mm, the interlocking of the base material with the cladding material is significantly less pronounced, which is possibly due to the lower degree of deformation in the area of the edge surface with greater weld-on thicknesses. The interface between the thicker material and the softer core is therefore more susceptible to shearing forces.

In Fig. 6 a (red circle (1)) and Fig. 6 b (red circle (2)), a dark area can be seen below the cladding layer. This area cannot be recognized in Fig. 6 c. When analyzing the hardness curves, it can be determined that in Fig. c is a pronounced decrease in hardness from approx. 700 HV in the coating material to approx. 200 HV in the base material. For the samples with 2.5 mm and 5 mm coating material, the hardness initially drops sharply from approx. 700 HV to approx. 350 HV. It then decreases more slowly to approx. 220 HV. This slower drop in hardness and the dark area are probably due to diffused carbon. The gradient in carbon concentration between the two alloys (Table 2) leads to the diffusion into C22.8. The presumably carburized zone is uneven in its thickness, being less pronounced in areas of thicker cladding. As diffusion is a primarily heat and time driven mechanism and the form of the layer appears to follow material flow, the carburized zone is most likely generated in the heating process prior to forming. During the forming process, the diffusion layer is concentrated in the teeth by the flowing material and displaced at the tooth roots. Higher cladding thicknesses result in less material flow into the tooth, which is why this effect is more recognizable with lower cladding thicknesses. Indirect heating in chamber furnaces is based on heat transfer from the furnace atmosphere into the outer billet surface before it is transported further into the core. The diffusion process is enhanced for thin cladding closer to the outer surface as higher temperatures are reached earlier and therefore held over a longer fraction of the 30 min heating time.

Light-colored areas can be seen in the surface layer at the tooth tip of all three samples, which extend into the tooth flanks. In b) and c), the tooth tip exhibits reduced hardness close to the surface, before reaching a plateau level. The absence of this hardness drop for 2.5 mm cladding in a) can be lead back to the limited thickness of the decarburized layer that is stretched and thinned out through the forming process and cannot be resolved with the applied HV1 hardness test load.

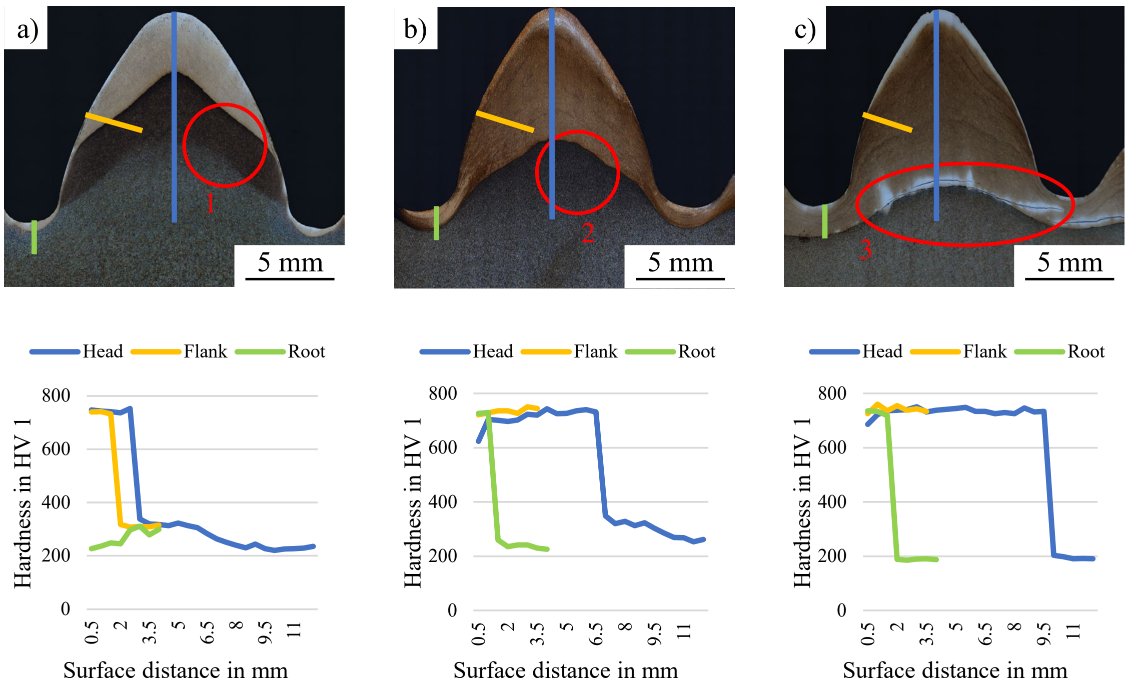

Figure 6 – Formed spur gears with cladding thicknesses of a) 2.5 mm (1: dark area), b) 5 mm (2: dark area), c) 7.5 mm (3: cracks) and the corresponding hardness curves

When comparing the contours of the forged components with the FE simulation results, it is detected that the results differ for thin claddings. The material flow of the base material into the tooth showed deviations for a thickness of 2.5 mm (Fig. 7 a). On the other hand, a high degree of agreement was achieved with increasing cladding thickness, as can be seen in Fig. 7 b. The cladding layer and the cladding interface to the base material is subjected to more extreme deformation and thinning for thinner layers. A strong thinning occurs between the tooth flank and the tooth root. This strong thinning is difficult to model numerically. In addition, numerical simulation of the damage behavior represents a separate area of research and the parametrization of a damage model would require additional investigations [18], damage effects were not considered for this study. The effects are especially enhanced by additional sources of uncertainty with limited modelling accuracy such as friction which is of major importance in forging.

The model applied here should therefore be limited to applications with higher cladding layer thickness as it shows good accordance to experimental results in this parameter space.

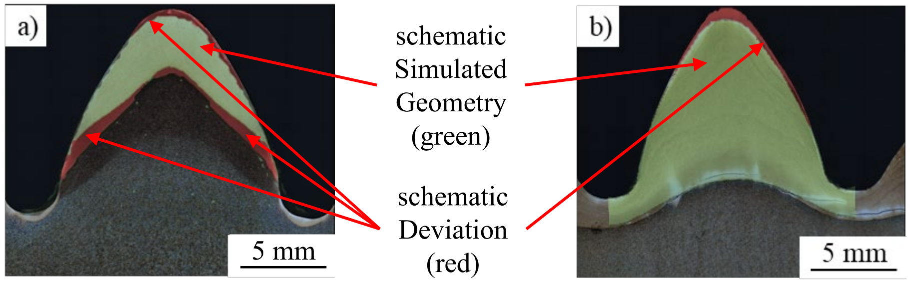

Figure 7 – Contour comparison of forging and simulation results for a) 2.5 mm and b) 7.5 mm weld thickness

Summary and outlook

In summary, the results show that the material flow in the teeth of a spur gear can be adjusted by varying the cladding thickness. Thin cladding layers have a significant influence on the material distribution in the component.

The supposed impact of carbon transfer on mechanical and performance properties is to be analyzed in further work. It can also be investigated whether this effect can be prevented by a faster inductive heating strategy.

Material flow predictions with the multi-material FE process model used here are possible from a certain layer thickness. A high degree of agreement between FE simulation and experimental results was detected with thick layers and minor deviations with thin layers. To investigate these deviations, a mesh study can be carried out to determine the properties of the elements and damage models can be implemented.

EDX analyses and nanoindenter measurements at the interface can be contribute to better understanding of the involved mechanisms. Based on these results, a virtual optimization of the material distribution in gear components through FE modelling is possible. Ideal results are expected by combining the developed model for gear production with simulation methods used to model load and damage distribution in gear applications.

Acknowledgements

Funded by the Deutsche Forschungsgemeinschaft (DFG, German Research Foundation) – CRC 1153 subproject B02 – 252662854.

References

[1] M. Ashby, Multi-objective optimization in material design and selection. *Acta materialia*, *48*(1) (2000) 359-369. https://doi.org/10.1016/S1359-6454(99)00304-3

[2] K. Martinsen, S. J. Hu, B. E. Carlson, Joining of dissimilar materials. *Cirp Annals*, *64*(2) (2015) 679-699. https://doi.org/10.1016/j.cirp.2015.05.006

[3] M. Merklein, M. Johannes, M. Lechner, A. Kuppert, A review on tailored blanks—Production, applications and evaluation. *Journal of Materials Processing Technology*, *214*(2) (2014) 151-164. https://doi.org/10.1016/j.jmatprotec.2013.08.015

[4] A. Carrad`o, O. Sokolova, G. Ziegmann, H. Palkowski, Press joining rolling process for hybrid systems. *Key Engineering Materials*, *425* (2010) 271-281. https://doi.org/10.4028/www.scientific.net/KEM.425.271

[5] D. W. Dudley, Zahnräder: Berechnung, Entwurf und Herstellung nach amerikanischen Erfahrungen, Springer, 1961. ISBN: 978-3-642-92804-8

[6] W. Wang, N. J. Politis, Y. Wang, X. Zhou, D. Balint, J. Jiang, Solid-state hot forge bonding of aluminium-steel bimetallic gears: deformation mechanisms, microstructure and mechanical

properties. *International Journal of Machine Tools and Manufacture*, *180* (2022) 103930. https://doi.org/10.1016/j.ijmachtools.2022.103930

[7] A. Chugreeva, M. Mildebrath, J. Diefenbach, A. Barroi, M. Lammers, J. Hermsdorf, T. Hassel, L. Overmeyer, B.-A. Behrens, Manufacturing of high-performance Bi-metal bevel gears by combined deposition welding and forging. *Metals*, *8*(11) (2018) 898. https://doi.org/10.3390/met8110898

[8] B.-A. Behrens, J. Diefenbach, A. Chugreeva, C. Kahra, S. Herbst, F. Nürnberger, Tailored forming of hybrid bevel gears with integrated heat treatment. *Procedia Manufacturing*, *47* (2020) 301-308. https://doi.org/10.1016/j.promfg.2020.04.234

[9] B.-A. Behrens, A. Chugreeva, J. Diefenbach, C. Kahra, S. Herbst, F. Nürnberger, H. J. Maier, Microstructural evolution and mechanical properties of hybrid bevel gears manufactured by tailored forming. *Metals*, *10*(10) (2020) 1365. https://doi.org/10.3390/met10101365

[10] L. Budde, P. Merkel, V. Prasanthan, S. Bährisch, M. Y. Faqiri, M. Lammers, M. Stonis, J. Hermsdorf, T. Hassel, J. Uhe, B.-A. Behrens, B. Breidenstein, L. Overmeyer, In Proceedings of the 33rd Annual International Solid Freeform Fabrication Symposium - An Additive Manufacturing Conference. (2022) 1223–1233. https://doi.org/10.1007/s00170-021-08066-3

[11] M. Bambach, I. Sizova, F. Kies, C. Haase, Directed energy deposition of Inconel 718 powder, cold and hot wire using a six-beam direct diode laser set-up. *Additive Manufacturing*, *47* (2021) 102269. https://doi.org/10.1016/j.addma.2021.102269

[12] A. Kisielewicz, K. Thalavai Pandian, D. Sthen, P. Hagqvist, M. A. Valiente Bermejo, F. Sikström, A. Ancona, Hot-wire laser-directed energy deposition: process characteristics and benefits of resistive pre-heating of the feedstock wire. Metals, 11(4) (2021) 634. https://doi.org/10.3390/met11040634

[13] DIN EN 10273: 2016, Warmgewalzte schweißgeeignete Stäbe aus Stahl für Druckbehälter mit festgelegten Eigenschaften bei erhöhten Temperaturen.

[14] Swiss Steel Holding AG Werkstoffdatenblatt X45CrSi9-3 1.4718 https://swisssteel-group.com/content-media/documents/Data-Sheets/Stainless-Steel/1.4718_de.pdf. Accessed 10 December 2024

[15] B. Behrens, J. Uhe, H. Wester, T. Matthias, C. Büdenbender, FE-based layer design of deposition-welded semi-finished parts for the production of hybrid bevel gear. *Procedia Manufacturing*, *47* (2020) 309-314. https://doi.org/10.1016/j.promfg.2020.04.235

[16] P. Merkel, L. Budde, K. Biester, Y. Faqiri, V. Prasanthan, P. Herrmann, B. A. Behrens, Production and Forming of Deposition-Welded Hybrid Multimaterial Shafts. *Advanced Engineering Materials*, (2024) 2401391. https://doi.org/10.1002/adem.202401391

[17] B. Denkena, B. A. Behrens, L. Overmeyer, S. Kaierle, B. Bergmann, H. Klemme, M. Handrup, Sensitivity of process signals to deviations in material distribution and material properties of hybrid workpieces. *The International Journal of Advanced Manufacturing Technology*, *130*(5), (2024) 2649-2659. https://doi.org/10.1007/s00170-023-12807-x

[18] A. E. Tekkaya, P.O. Bouchard, S. Bruschi, C.C. Tasan, Damage in metal forming, *CIRP Annals*, *69*(2) (2020) 600-623. https://doi.org/10.1016/j.cirp.2020.05.005